# Juvenile CLN3 disease is a lysosomal cholesterol storage disorder: similarities with Niemann-Pick type C disease

Jacinda Chen,[a] Rajesh Kumar Soni,[b] Yimeng Xu,[c] Sabrina Simoes,[a,d] Feng-Xia Liang,[e] Laura DeFreitas,[c] Robert Hwang, Jr.[a] Jorge Montesinos,[d,j] Joseph H. Lee,[a,d,f,g] Estela Area-Gomez,[a,d,h,j] Renu Nandakumar,[c] Badri Vardarajan,[a,d,f] and Catherine Marquer[a,i,*]

[a]Taub Institute for Research on Alzheimer's Disease and the Aging Brain, Columbia University Irving Medical Center, New York City, NY 10032, USA
[b]Proteomics and Macromolecular Crystallography Shared Resource, Herbert Irving Comprehensive Cancer Center, New York City, NY 10032, USA
[c]Biomarkers Core Laboratory, Irving Institute for Clinical and Translational Research, Columbia University Irving Medical Center, New York City, NY 10032, USA
[d]Department of Neurology, Columbia University Irving Medical Center, New York City, NY 10032, USA
[e]Microscopy Core Laboratory of Division of Advanced Research Technologies, New York University Grossman School of Medicine, New York City, NY 10016, USA
[f]G. H. Sergievsky Center, Columbia University Irving Medical Center, New York City, NY 10032, USA
[g]Department of Epidemiology, Columbia University Irving Medical Center, New York City, NY 10032, USA
[h]Institute of Human Nutrition, Columbia University Irving Medical Center, New York City, NY 10032, USA
[i]Department of Pathology and Cell Biology, Columbia University Irving Medical Center, New York City, NY 10032, USA

eBioMedicine
2023;92: 104628
Published Online 26 May 2023
https://doi.org/10.1016/j.ebiom.2023.104628

## Summary

**Background** The most common form of neuronal ceroid lipofuscinosis (NCL) is juvenile CLN3 disease (JNCL), a currently incurable neurodegenerative disorder caused by mutations in the *CLN3* gene. Based on our previous work and on the premise that CLN3 affects the trafficking of the cation-independent mannose-6 phosphate receptor and its ligand NPC2, we hypothesised that dysfunction of CLN3 leads to the aberrant accumulation of cholesterol in the late endosomes/lysosomes (LE/Lys) of JNCL patients' brains.

**Methods** An immunopurification strategy was used to isolate intact LE/Lys from frozen autopsy brain samples. LE/Lys isolated from samples of JNCL patients were compared with age-matched unaffected controls and Niemann–Pick Type C (NPC) disease patients. Indeed, mutations in *NPC1* or *NPC2* result in the accumulation of cholesterol in LE/Lys of NPC disease samples, thus providing a positive control. The lipid and protein content of LE/Lys was then analysed using lipidomics and proteomics, respectively.

**Findings** Lipid and protein profiles of LE/Lys isolated from JNCL patients were profoundly altered compared to controls. Importantly, cholesterol accumulated in LE/Lys of JNCL samples to a comparable extent than in NPC samples. Lipid profiles of LE/Lys were similar in JNCL and NPC patients, except for levels of bis(monoacylglycero) phosphate (BMP). Protein profiles detected in LE/Lys of JNCL and NPC patients appeared identical, except for levels of NPC1.

**Interpretation** Our results support that JNCL is a lysosomal cholesterol storage disorder. Our findings also support that JNCL and NPC disease share pathogenic pathways leading to aberrant lysosomal accumulation of lipids and proteins, and thus suggest that the treatments available for NPC disease may be beneficial to JNCL patients. This work opens new avenues for further mechanistic studies in model systems of JNCL and possible therapeutic interventions for this disorder.

**Funding** San Francisco Foundation.

**Copyright** © 2023 The Author(s). Published by Elsevier B.V. This is an open access article under the CC BY-NC-ND license (http://creativecommons.org/licenses/by-nc-nd/4.0/).

*Corresponding author. Taub Institute for Research on Alzheimer's Disease and the Aging Brain, Columbia University Irving Medical Center, New York City, NY 10032, USA.
*E-mail address:* cm3244@cumc.columbia.edu (C. Marquer).
[i]Current address: Department of Cellular and Molecular Biology, Centro de Investigaciones Biológicas Margarita Salas, CSIC, Madrid 28040, Spain.

Keywords: Juvenile CLN3 disease; Lysosomes; Niemann–Pick type C disease; Human brain tissue; Cholesterol; Proteomics

## Research in context

### Evidence before this study

Providing therapeutic options for juvenile CLN3 disease (JNCL), the most common neurodegenerative disease of childhood, is an important endeavour. The exact function of the enigmatic CLN3 protein impacted in JNCL pathogenesis is still a matter of debate. There is converging evidence that CLN3 plays a functional role in the trafficking of the cation-independent mannose-6 phosphate receptor (CI-M6PR) and its ligand NPC2; and we have independently shown that altering the CI-M6PR/NPC2 trafficking results in aberrant accumulation of cholesterol in the late endosomes/lysosomes (LE/Lys) compartment. On November 14th, 2022, we searched PubMed and Google Scholar with the keywords "juvenile CLN3 disease", "juvenile Batten disease", "Batten disease", "neuronal ceroid lipofuscinosis" and "Spielmeyer-Vogt disease". We found no studies comparing the lipid and protein profiles of LE/Lys compartments isolated from human autopsy brain samples of juvenile CLN3 disease patients to age-matched unaffected controls.

### Added value of this study

To capture a direct snapshot of human disease-relevant LE/Lys dysfunction, this study analysed the lipidomic and proteomic profiles of LE/Lys compartments isolated from frozen autopsy cortex samples of unaffected controls and juvenile CLN3 disease (JNCL) patients. As Niemann-Pick type C (NPC) disease is a known lysosomal cholesterol storage disorder, LE/Lys samples from NPC disease patients were conjointly analysed. We found major differences in the lipid and protein profiles of JNCL LE/Lys compared to controls as well as NPC LE/Lys compared to controls, as expected. However, one of our main findings is that LE/Lys from JNCL and NPC samples were surprisingly similar, both at the lipid and protein level. Another key finding is that cholesterol accumulates to a similar extent in JNCL and NPC LE/Lys.

### Implications of all the available evidence

Taken together, the evidence supports that JNCL is a lysosomal cholesterol storage disorder, with unsuspected similarities with NPC disease. First, we expect that the lipid and protein datasets from human samples provided here will be further mined to establish a strong foundation for future mechanistic studies in model systems of JNCL. We also expect that these datasets will be used as a reference when assessing LE/Lys dysfunction in other lysosomal storage disorders and neurodegenerative diseases of aging. Finally, the unsuspected lipid and protein similarities between JNCL and NPC support that these disorders may share pathogenic pathways, and thus that treatments available for NPC may be beneficial to JNCL patients.

## Introduction

The neuronal ceroid lipofuscinoses (NCLs) are a group of fatal inherited neurodegenerative disorders that share similar clinical features, such as visual failure, seizures, progressive decline in cognitive and motor abilities as well as accumulation of autofluorescent storage material.[1–3] However, they differ widely in the age of onset, ranging from infantile to adult, as well as in the nature of the first symptoms presented by the patients. Mutations in over a dozen genes have been linked to NCLs and provide the basis for the current nomenclature of these disorders.[4] The most common NCL is juvenile CLN3 disease (JNCL), a disorder caused by mutations in the *CLN3* gene.[5] Although a large number of mutations have been identified in *CLN3*,[3] the most common disease-causing alteration is a 1-kb deletion. JNCL usually presents first with vision loss around 4–7 years of age, followed by changes in cognition and behaviour, seizures and psychomotor decline leading to an early death in the early twenties.[6] CLN3 is a putative lysosomal transmembrane protein associated with roles in endocytosis, cargo sorting and trafficking, lysosomal function, autophagy, $Ca^{2+}$ signalling and osmoregulation.[7,8] The exact pathways in which CLN3 plays a functional role vs. processes affected as a secondary consequence, as well as the nature of the pathways affected by the 1-kb deletion causing JNCL, are still a matter of controversy. These unanswered questions may in part explain why there is currently no treatment available for this fatal disorder.

Evidence collected in cellular model systems of JNCL points to a role of CLN3 in the correct intracellular trafficking of the cation-independent mannose-6 phosphate receptor (CI-M6PR).[9–11] CI-M6PR binds its ligands, mostly soluble lysosomal proteins, in the trans-Golgi network (TGN) and transports them to the endosomes. There, ligands will be released due to a lower pH and passively transported to the late endosomes/lysosomes (LE/Lys) where they can exert their function. Importantly, one of the ligands of CI-M6PR is NPC2,[12] and it has been reported that NPC2 is decreased in LE/Lys of JNCL cellular models.[10] In LE/Lys, endocytosed free cholesterol, hereafter referred to as cholesterol, is believed to be transferred by NPC2 from the LE/Lys lumen to the polytopic membrane protein NPC1. The latter then mediates the egress of cholesterol from the endolysosomal system, allowing for its distribution to other cellular compartments.[13] Remarkably, we have

previously reported that mistrafficking of CI-M6PR and its ligand NPC2 results in accumulation of cholesterol in LE/Lys.[14]

We thus hypothesised that JNCL may in fact be a lysosomal cholesterol storage disorder. To test whether cholesterol accumulates in the LE/Lys of JNCL patients, we used frozen human autopsy brain samples from JNCL patients and age-matched controls. Samples from patients with Niemann–Pick Type C (NPC) disease -in which mutations in *NPC1* or *NPC2* result in the accumulation of cholesterol in the LE/Lys[15]–were used as positive control. As the presence of autofluorescent pigments precludes the use of direct imaging of cholesterol, we used an immunopurification strategy to isolate LE/Lys from frozen brain samples and analysed their lipid and protein content using lipidomics and proteomics, respectively. We found that the lipid profiles of JNCL and NPC LE/Lys were profoundly altered compared to controls, and that both displayed a cholesterol increase. Intriguingly, we also observed that the protein signature of JNCL LE/Lys was essentially indistinguishable from NPC. Taken together, our results support that JNCL is a previously unrecognised lysosomal cholesterol storage disorder with unsuspected similarities with NPC disease, opening new avenues for further mechanistic studies and therapeutic interventions.

## Methods

### Reagents

Bovine serum albumin (BSA), anhydrous NaH2PO4 and Na2HPO4, sodium chloride NaCl, mannitol, HEPES and EGTA were from Sigma–Aldrich. $Ca^{2+}$ and $Mg^{2+}$ free phosphate buffered saline (PBS) was from Gibco. EDTA was from J.T. Baker. $BS^3$ Crosslinker was from Pierce and $BS^3$ Quenching Buffer (1 M Tris HCl, pH 7.5) was from Fisher.

### Antibodies

The antibodies were obtained from the following sources: rabbit antibodies for LAMP1 [Abcam Cat# ab24170, RRID:AB_775978, 10 μg at 1 mg/mL for immunoprecipitation (IP) and 1/250 for western blot (WB)], Rab5A (Cell Signaling Technology Cat# 3547, RRID:AB_2300649, 1/1000 for WB), Sec61β (Thermo Fisher Scientific Cat# PA3-015, RRID:AB_2239072, 1/5000 for WB), Aquaporin 1 (Millipore Cat# AB2219, RRID:AB_1163380, 1/500 for WB) and ANKS1B (Proteintech Cat# 24783-1-AP, RRID:AB_2879720, 1/1000 for WB) and mouse antibody for ATP5A1 (Thermo Fisher Scientific Cat# 459,240, RRID:AB_2532234, 1/1000 for WB). Peroxidase-conjugated secondary antibodies were from Bio-Rad.

### Human brain tissues

Frozen samples from the dorsolateral prefrontal cortex (Brodmann Area 9) were obtained from Niemann-Pick disease type C (NPC), juvenile neuronal ceroid lipofuscinosis (JNCL) and age-matched non-affected control subjects (Supplementary Table S1). All samples were obtained from the NIH NeuroBioBank. Control cases were unaffected individuals who died from accidental causes. The number of independent biological replicates per condition was estimated by power analysis (G*power), based on an estimation of differences in cholesterol levels. Based on the treatise on power analysis,[16] we set the α-error (false-positive) ≤5% and β-error (false-negative) ≤20%. We have also considered that, based on pilot experiments, differences between means would have to be ≥20% to reflect meaningful differences and have used our historic data (means, SEMs) and the literature to estimate the error. The normality and homogeneity of variances were tested with Shapiro–Wilk test and F test, respectively. The mean ages at death and post-mortem delays of control cases and JNCL patients were not significantly different. Average age at death was 23.0 ± 1.6 and 24.8 ± 1.2 years for control (n = 6) and JNCL (n = 5) cases, respectively (p = 0.41, unpaired Student's t-test). Average post-mortem delays were 8.7 ± 0.3 h and 8.6 ± 2.3 h for control and JNCL cases (p = 0.97, unpaired t-test with Welch's correction). There were small differences between control cases and NPC patients as we were limited by the availability of frozen samples. Average age at death was 23.0 ± 1.6 and 16.8 ± 2.0 years for control (n = 6) and NPC (n = 4) cases, respectively (p = 0.04, unpaired Student's t-test). Average post-mortem delays were 8.7 ± 0.3 h and 18.5 ± 3.8 h for control and NPC cases and were not significantly different (p = 0.08, unpaired t-test with Welch's correction). Both males and females were used for this study. There were only Caucasian samples available for this study.

For some samples, the presence of mutations in *CLN3* had previously been tested and results were available from the NIH NeuroBioBank records. For the others, we assessed whether JNCL patients were indeed carriers of *CLN3* mutations/deletions. Briefly, DNA was extracted from 15 to 25 mg of frozen brain tissue with the Qiagen QIAamp Fast DNA Tissue Kit and its quantity and quality assessed with Nanodrop. Twist Biosciences Whole Exome library prep was completed using their Comprehensive Human exome probe panel. Whole Exome sequencing was performed using the Twist design library of 39 Mb to achieve 60 × coverage for all samples. We aligned the WES reads to the human reference genome build 38 using the Burrows Wheeler Aligner (http://bio-bwa.sourceforge.net/). Quality control of the sequencing data was done using established methods, including base alignment quality calibration and refinement of local alignment around putative indels using the Genome Analysis Toolkit (GATK). Variants were called and recalibrated using multi-sample calling with GATK's HaplotypeCaller and GenotypeGVCF modules. Reliably called variants were annotated by ANNOVAR. Depth of coverage analysis

identified a *CLN3* syndromic deletion in the JNCL samples (Supplementary Fig. S1). An unaffected control and a sample with non-synonymous variants in *CLN2* were analysed alongside the JNCL samples and as expected, did not carry the *CLN3* deletion. Presence of the common 1-kb deletion was confirmed by PCR, as described in.[17]

### Ethics

The project was reviewed and approved by the NIH NeuroBioBank. The project was classified as Not Human Subjects Research Under 45 CFR 46 by the institutional review boards of the Columbia University Irving Medical Center (AAAT7076).

### Human brain tissue homogenisation

All steps of brain tissue homogenisation were performed on ice. Approximately 500 mg of frozen brain tissue was minced with a razor blade before being transferred to a Potter-Elvenhjem Teflon-pestle grinder (PYREX) and homogenised with 10 mL/g of ice-cold homogenisation buffer (HB, 225 mM mannitol, 25 mM HEPES-KOH, 1 mM EGTA), filtered (0.2 µM Stericup filter, Millipore) and supplemented with cOmplete Protease Inhibitors (Roche) beforehand. The resulting brain homogenate was transferred to 1.5 mL tubes (Eppendorf) and centrifuged at 1500×*g* at 4 °C for 10 min, giving Supernatant 1 ($Sup_1$) and Pellet 1 ($P_1$). The $P_1$ pellet was further resuspended with 1 mL of HB and centrifuged again at 1500×*g* at 4 °C for 10 min to obtain more Supernatant 1 ($Sup_1$). All $Sup_1$ samples were then centrifuged at 1500×*g* at 4 °C for 10 min. The resulting Supernatant 2 ($Sup_2$) samples were centrifuged at 16,000×*g* at 4 °C for 15 min, to give Pellet 3 ($P_3$). All membrane-rich pellets $P_3$ were pooled and resuspended in 500 µL of HB. This solution is hereafter referred to as the membrane fraction (MF). The protein content of the MF was analysed by protein dosage (BCA, Pierce) and 500 µg of proteins were used to isolate LE/Lys.

### Isolation of LE/Lys from human brain tissue homogenate

LE/Lys were isolated from brain homogenate by immunoprecipitation (IP) with a LAMP1 antibody (Abcam) crosslinked to M–280 Sheep Anti-Rabbit IgG Dynabeads (Invitrogen). Dynabeads were prepared as suggested by the manufacturer. Briefly, Dynabeads were first resuspended by vortexing them for 45 s. For two IPs, 200 µL of Dynabeads were washed with 1 mL ice-cold Washing Buffer ($Ca^{2+}$- and $Mg^{2+}$- free PBS, 0.1% BSA, 2 mM EDTA, pH 7.4) with tilting and rotation (Boekel rotator) for 5 min at room temperature. The beads were placed on a Dynamag-2 magnet (Invitrogen) for 1 min, and the solution discarded. This step was repeated once more with 1 mL washing buffer. The beads were then washed with 800 µL Conjugation buffer (20 mM Sodium Phosphate, 0.15 M NaCl, pH 7) with tilting and rotation for 5 min at room temperature. The beads were placed on the magnet for 1 min, and the solution discarded. This step was repeated once more with 800 µL Conjugation buffer. The beads were then resuspended in 1 mL of freshly prepared $BS^3$ Crosslinker solution (5 mM $BS^3$ in Conjugation Buffer, Pierce) supplemented with 20 µg LAMP1 rabbit antibody (Abcam) and incubated with tilting and rotation for 30 min at room temperature. After 30 min, the crosslinking reaction was quenched by the addition of 50 µL of quenching buffer (1 M Tris HCl, pH 7.5) and further incubation with tilting and rotation for 30 min at room temperature. The crosslinked beads were then placed on the magnet for 1 min, and the supernatant discarded. The crosslinked beads were washed three times with 800 µL PBS and tilting/rotation for 5 min at room temperature. After these washes, crosslinked beads were placed on the magnet for 1 min, and the supernatant discarded. The beads were then resuspended in 200 µL PBS.

For each IP, 100 µL of freshly prepared LAMP1 antibody-crosslinked beads were incubated with 500 µg of brain membrane fraction diluted in 100 µL PBS with tilting and rotation for 3 h at 4 °C.

After the incubation, the beads were placed on the magnet for 2 min, and the supernatant was saved (Supernatant a, $Sup_a$). The beads were then washed with 1 mL Washing Buffer with tilting and rotation for 5 min at room temperature. The beads were placed on the magnet for 2 min, and the supernatant saved ($Sup_b$). This step was repeated once more, resulting in Supernatant c ($Sup_c$). Finally, the beads were resuspended in 100 µL of PBS complemented with cOmplete protease inhibitors (Roche) and assayed for western blot, electron microscopy, lipidomics or proteomics.

### Protein biochemistry and immunoblotting

To assess the quality of the IP, we ran input, supernatant and pellet samples. Input samples consisted of 10 µL of brain membrane fraction diluted 1/10 in PBS supplemented with cOmplete protease inhibitors (Roche). Supernatant samples consisted of 10 µL of $Sup_a$ and pellet samples consisted of 10 µL of resuspended beads. To validate our proteomics hits, we ran pellet samples consisting of 10 µL of resuspended beads. Samples were prepared with NuPAGE Sample Reducing Agent (Invitrogen) and NuPAGE LDS Sample Buffer (Invitrogen). Input samples underwent an additional step of sonication in a water bath sonicator for 10 min. All samples were placed at 70 °C for 10 min, centrifuged for 1 min at 16,000×*g* and transferred to the magnet for 2 min. The resulting solution was loaded in the gel. SDS–PAGE was performed on samples loaded in NuPAGE 4–12% Bis-Tris gels (Life technologies). Wet transfer was performed at 80 V for 1 h 45 min at 4 °C (Bio-Rad). Primary and secondary antibodies were

incubated overnight at 4 °C and 1 h at room temperature, respectively. Revelation was performed with Immobilon Western Chemiluminescent HRP Substrate (EMD Millipore) and the chemiluminescent signal was imaged with ImageQuant LAS4000 mini (GE Healthcare). Quantification was performed with ImageJ software.

### Transmission electron microscopy

10 µL of resuspended beads were fixed overnight with 2% paraformaldehyde (Electron Microscopy Sciences) in 0.2 M Phosphate buffer at 4 °C. The suspension was loaded onto formvar–carbon-coated EM grids (FCF-100-CU, Electron Microscopy Sciences) and fixed a second time with 1% glutaraldehyde (Electron Microscopy Sciences) for 5 min. After 8 washes with MilliQ water, samples were contrasted and embedded in a mixture of 1 V uranyl acetate and 9 V methylcellulose (Electron Microscopy Sciences), before being visualised at the microscope. Stained grids were examined using a transmission electron microscope (FEI Talos 120 °C) and photographed with a Gatan OneView 4-k × 4-k camera (Gatan, Inc.).

### Lipidomics

Lipidomic profiling was performed on samples from control individuals (n = 6), JNCL patients (n = 5) and NPC patients (n = 3) using Ultra Performance Liquid Chromatography-Tandem Mass Spectrometry (UPLC-MS/MS).[18,19] Briefly, lipid extracts were prepared from 80 µL of resuspended beads spiked with appropriate internal standards using a modified Bligh and Dyer method, and analysed on a platform comprising Agilent 1260 Infinity HPLC integrated to Agilent 6490 A QQQ mass spectrometer controlled by Masshunter v 7.0 (Agilent Technologies). Beads were removed by incubation on the magnet for 2 min after lipid extraction. Glycerophospholipids and sphingolipids were separated with normal-phase HPLC as described before,[20] with a few modifications. An Agilent Zorbax Rx-Sil column (2.1 mm internal diameter, 100 mm length, 1.8 µm particle size) maintained at 25 °C was used under the following conditions: mobile phase A (chloroform: methanol: ammonium hydroxide, 89.9:10:0.1, v/v) and mobile phase B (chloroform: methanol: water: ammonium hydroxide, 55:39:5.9:0.1, v/v); 95% A for 2 min, decreased linearly to 30% A over 18 min and further decreased to 25% A over 3 min, before returning to 95% over 2 min and held for 6 min. Separation of sterols and glycerolipids was carried out on a reverse phase Agilent Zorbax Eclipse XDB-C18 column (4.6 mm internal diameter, 100 mm length, 3.5 µm particle size) using an isocratic mobile phase, chloroform, methanol, 0.1 M ammonium acetate (25:25:1) at a flow rate of 300 µL/min. Quantification of lipid species was accomplished using multiple reaction monitoring (MRM) transitions[20–22] under both positive and negative ionisation modes in conjunction with referencing of appropriate internal standards: PA 14:0/14:0, PC 14:0/14:0, PE 14:0/14:0, PG 15:0/15:0, PI 17:0/20:4, PS 14:0/14:0, BMP 14:0/14:0, APG 14:0/14:0, LPC 17:0, LPE 14:0, LPI 13:0, Cer d18:1/17:0, SM d18:1/12:0, dhSM d18:0/12:0, GalCer d18:1/12:0, GluCer d18:1/12:0, LacCer d18:1/12:0, D7-cholesterol, CE 17:0, MG 17:0, 4 ME 16:0 diether DG, D5-TG 16:0/18:0/16:0 (Avanti Polar Lipids). Lipid levels for each sample were calculated by summing the total number of moles of all lipid species measured by all three LC-MS methodologies, and then normalising the total to mol%. The final data are presented as mean mol%.

Lipid abbreviations are as follows: (FC) Free Cholesterol, (CE) Cholesterol Ester, (AC) Acyl Carnitine, (MG) Monoacylglycerol, (DG) Diacylglycerol, (TG) Triacylglycerol, (Cer) Ceramide, (dhCer) Dihydroceramide, (SM) Sphingomyelin, (dhSM) Dihydrosphingomyelin, (Sulf) Sulfatide, (MHCer) Monohexosylceramide (galactosylceramide + glucosylceramide), (LacCer) Lactosylceramide, (GM3) Monosialodihexosylganglioside, (GB3) Globotriaosylceramide, (PA) Phosphatidic acid, (PC) Phosphatylcholine, (PCe) Ether phosphatidylcholine, (PE) Phosphatidylethanolamine, (PEp) Plasmalogen phosphatidylethanolamine, (PS) Phosphatidylserine, (PI) Phosphatidylinositol, (PG) Phosphatidylglycerol, (BMP) Bis(monoacylglycero)phosphate, (AcylPG) Acyl Phosphatidylglycerol, (LPC) Lysophosphatidylcholine, (LPCe) Ether lysophosphatidylcholine, (LPE) Lysophosphatidylethanolamine, (LPEp) Plasmogen Lysophosphatidylethanolamine, (LPI) Lysophosphatidylinositol, (LPS) Lysophosphatidylserine, (NAPE) N-Acyl Phosphatidylethanolamine, (NAPS) N-Acyl Phosphatidylserine, (NSer) N-Acyl Serine.

### Proteomics

Proteomic profiling was performed on samples from control individuals (n = 6), JNCL patients (n = 5) and NPC patients (n = 4). Samples consisting of 80 µL of pelleted beads were prepared for tandem mass spectrometry (LC-MS/MS) by on beads digestion. Immunoprecipitated proteins on magnetic beads were washed five times with 200 µL of 100 mM Tris-pH 8.0. Proteins were reduced with 10 mM TCEP and alkylated with 11 mM iodoacetamide (IAA) that was quenched with 5 mM DTT. Protein digestion was processed by adding 1 µg of trypsin/LysC mix overnight at 37 °C and 1400 rpm. The next day, digested peptides were collected in a new microfuge tube and digestion was stopped by the addition of 1% TFA (final v/v), followed by centrifugation at 14,000×g for 10 min at room temperature. Cleared digested peptides were desalted on a SDB-RPS Stage-Tip[23] and dried in a speed-vac. Peptides were dissolved in 3% acetonitrile/0.1% formic acid.

Peptide concentrations were determined using NanoDrop and 200 ng of each sample were used for diaPASEF[24] analysis on timsTOFPro. Peptides were

separated within 87 min at a flow rate of 400 nl/min on a reversed-phase C18 column with an integrated CaptiveSpray Emitter (25 cm × 75 µm, 1.6 µm, IonOpticks). Mobile phases A and B were with 0.1% formic acid in water and 0.1% formic acid in ACN. The fraction of B was linearly increased from 2 to 23% within 60 min, followed by an increase to 35% within 7 min and a further increase to 90% before re-equilibration. The timsTOF Pro was operated in diaPASEF mode[24] and data was acquired at defined 32 × 50 Th isolation windows from $m/z$ 400 to 1200. The collision energy was ramped linearly as a function of the mobility from 59 eV at 1/K0 = 1.6 Vs cm$^{-2}$ to 20 eV at 1/K 0 = 0.6 Vs cm$^{-2}$.

### Statistics and data analysis

For lipidomics, statistical analysis was performed using GraphPad Prism software (version 9.2.0). Data was analysed using multiple unpaired t-tests with Welch's correction with a p value threshold of 0.05. Mol% values were averaged per disease group, and values of log2 fold change compared to controls were used to generate heatmaps.

For proteomics, the acquired diaPASEF raw files were searched with the UniProt Human proteome database (UP000005640) in the DIA-NN search engine with default settings of the library-free search algorithm.[25] Our predicted library contained 20,329 proteins and 20,121 genes. The false discovery rate (FDR) was set to 1% at the peptide precursor and protein level.[25] Area under the peaks were quantified using the MaxLFQ algorithm embedded in DIA-NN. Results obtained from DIA-NN were then exported and further analysed using Perseus software.[26] Quantified values were log2 transformed. Proteins quantified in at least three samples per disease group constituted a first dataset of "detected proteins" and were used for Venn diagram analysis. Representation was generated with https://bioinformatics.psb.ugent.be/webtools/Venn/. Another dataset of "differentially expressed proteins" was generated by comparing proteins that were detected in both groups being compared. Significantly changed protein abundance was determined by multiple t-tests with a threshold for significance of $p < 0.05$ (with a permutation-based FDR correction) using Perseus. Only proteins that (i) were upregulated or downregulated by more than 1·5 fold change (FC) (i.e., ≥0.58 or ≤ –0.58 in log2 FC) and (ii) were identified based on ≥1 "unique" peptide and ≥2 "unique + shared" peptides were kept for further analysis. Heatmaps were generated with GraphPad Prism software (version 9.2.0). Gene Ontology analysis was performed with ShinyGO 0.77.[27] Pathway analysis was performed with reactome.org version 82.[28]

### Role of funders

The funding source had no involvement in the collection, analysis and interpretation of the data, nor in the writing of the manuscript.

## Results

### Characterisation of LE/Lys isolated from frozen human autopsy brain samples

We isolated LE/Lys compartments from frozen human prefrontal cortex tissue (Supplementary Table S1 and Supplementary Fig. S1), using a combination of homogenisation, centrifugation and immunoprecipitation with an antibody directed against the LE/Lys protein LAMP1 conjugated to magnetic beads. Isolated compartments were characterised by western blot analysis, as well as transmission electron microscopy (TEM). Using western blot analysis, we observed that the immunoprecipitated pellets contained LAMP1 protein but not markers of early endosomes, endoplasmic reticulum or mitochondria (Supplementary Fig. S2a). Further, using TEM, we observed that these pellets contained vesicles of about 300 nm in diameter filled with electron dense material, in line with the expected morphology of intact LE/Lys compartments (Supplementary Fig. S2b). In addition, when performing proteomics analysis of the isolated LE/Lys (see the corresponding section), we could detect both lysosomal integral membrane proteins and soluble proteins, supporting that LE/Lys had been isolated intact (Supplementary Table S2).

### Cholesterol accumulates in the LE/Lys of JNCL patients

We then analysed LE/Lys isolated from JNCL and NPC patients using lipidomics and compared them with age-matched unaffected controls. As illustrated in Fig. 1, Supplementary Fig. S3 and Supplementary Table S3, the lipid profiles of JNCL and NPC patients were vastly different from that of the controls. Interestingly, LE/Lys from JNCL and NPC patients showed similarities in their lipid profiles. Indeed, out of 34 lipid classes, 7 classes differed from control samples in both JNCL and NPC patients and they were affected in the same direction. Cholesterol (FC) and monosialodihexosylganglioside (GM3) were upregulated, while phosphatidylcholine (PC), ether phosphatidylcholine (PCe), sphingomyelin (SM), phosphatidylethanolamine (PE) and phosphatidylserine (PS) were downregulated in JNCL and NPC samples compared to controls. The cholesterol content of LE/Lys was increased by 31% in JNCL samples compared to controls, reminiscent of the increase observed in NPC samples (34%).

JNCL samples showed additional differences from the controls, specifically a downregulation of ceramides (Cer) and phosphatidylglycerol (PG). NPC samples also showed additional differences from the controls, such as an upregulation of ether lysophosphatidylcholine (LPCe) and N-Acyl Serine (NSer) and a downregulation of plasmalogen phosphatidylethanolamine (PEp) and phosphatidylinositol (PI). Rather strikingly, there were minimal statistically significant differences between the lipid profiles of JNCL and NPC LE/Lys samples; the only

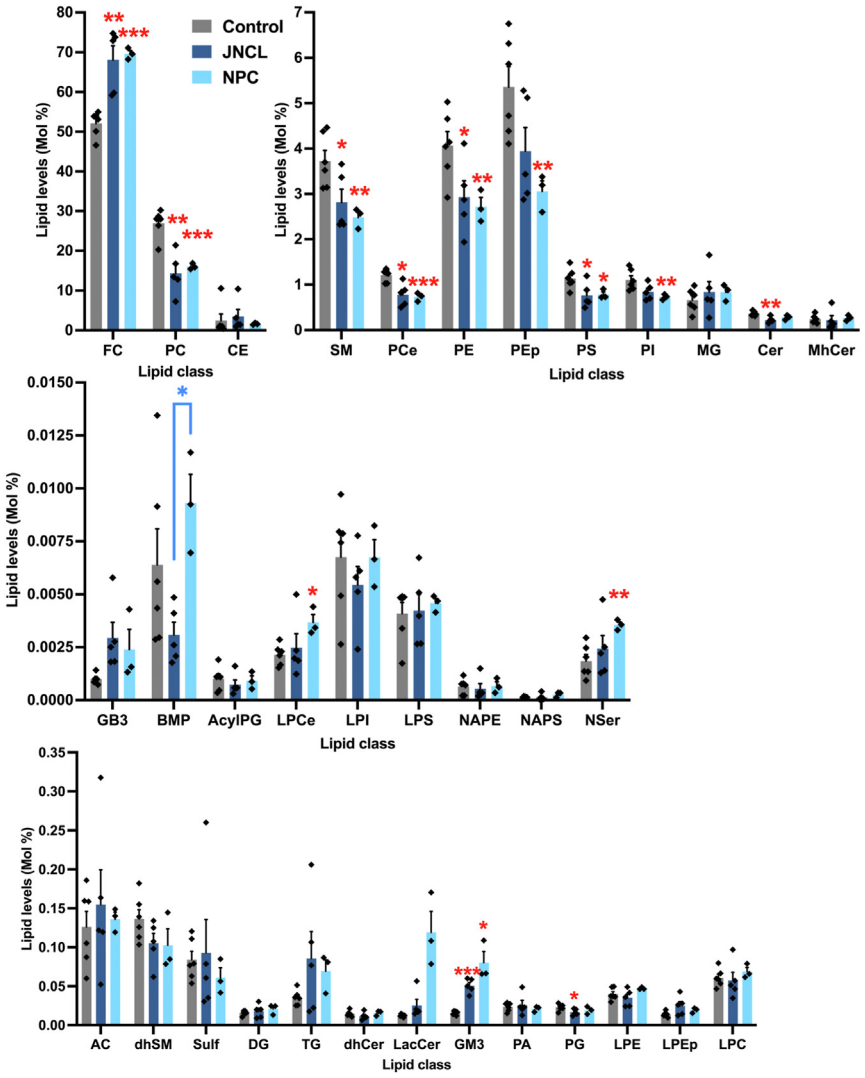


***Fig. 1:* Lipidomic profiling of LE/Lys isolated from brain tissue of JNCL, NPC and control individuals.** Quantification of 34 lipid classes by LC-MS/MS. Grey bars: controls (n = 6 individuals); dark blue bars: JNCL (n = 5 individuals); light blue bars: NPC (n = 3 individuals). *, ** and *** stand for $p < 0.05$, $p < 0.01$ and $p < 0.001$ in multiple unpaired t-tests with Welch's correction, respectively. Red asterisks indicate comparisons with controls, while blue asterisks indicate comparisons between JNCL and NPC. All values are given as mean ± s.e.m.

one being that there was less bis(monoacylglycero) phosphate (BMP) in JNCL samples.

We thus demonstrated that there is indeed a cholesterol increase in the LE/Lys of JNCL patients, in good accordance with our primary hypothesis.

## Proteomic profiles of JNCL and NPC LE/Lys are similar

Intrigued by the similarities in lipid profiles that we observed between JNCL and NPC samples, we decided to perform a proteomic analysis of LE/Lys samples from JNCL, NPC and control individuals to test whether similarities extended to the protein level.

We were able to detect over 6000 proteins in all LE/Lys samples: 6363 in controls, 6452 in JNCL and 6167 in NPC samples (Fig. 2). Most of these proteins (5972) were detected in all conditions, allowing us to perform a robust comparative analysis of LE/Lys protein profiles. In addition, 251 proteins were shared between JNCL and controls; 39 between NPC and controls and 139 between JNCL and NPC. There were only 101, 90 and 17 proteins detected only in controls, JNCL and NPC, respectively.

We first focused on the 90 proteins identified only in JNCL LE/Lys samples (Supplementary Table S4). Gene Ontology (GO) enrichment analysis revealed that the

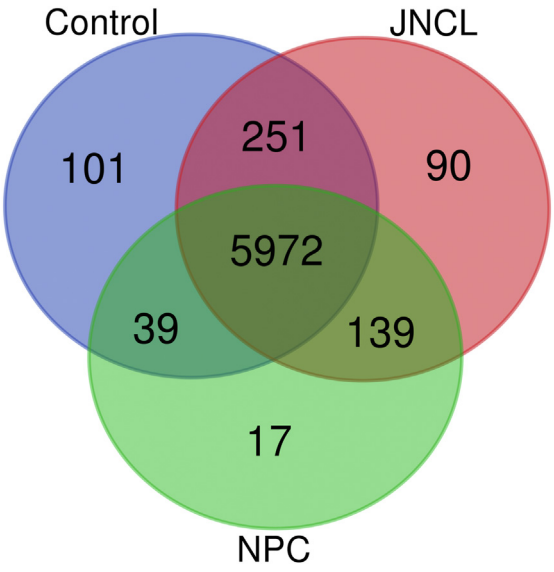


***Fig. 2:* Venn diagram of unique and shared proteins detected in LE/Lys isolated from brain tissue of JNCL, NPC and control individuals.** Blue: controls (n = 6 individuals); red: JNCL (n = 5 individuals); green: NPC (n = 4 individuals). Representation was generated with https://bioinformatics.psb.ugent.be/webtools/Venn/.

most significant enrichment was observed for biological pathways of growth hormone receptor signalling pathway, cellular response to growth hormone stimulus and growth hormone receptor signalling pathway via JAK-STAT. At the molecular function level, pathways of growth hormone receptor binding and hormone receptor binding were significantly enriched. Kyoto Encyclopaedia of Genes and Genomes (KEGG) pathway analysis indicated significant enrichment in the PI3K-Akt signalling pathway.

We then analysed the proteins that were differentially expressed between groups. Some of our hits were confirmed by western blot (Supplementary Fig. S4). Ankyrin Repeat and Sterile Alpha Motif Domain Containing 1 B (ANKS1B, also called amyloid precursor protein intracellular domain associated-1 protein or AIDA-1) is a scaffold protein of the postsynaptic density with roles in synaptic plasticity.[29,30] In our proteomics results, ANKS1B was downregulated in LE/Lys samples of JNCL patients compared to controls as well as in samples of NPC patients compared to controls. This depletion was confirmed using western blot. We also validated our methodology. The filter we used to identify differentially expressed proteins required 1 "unique" peptide and 2 "unique and shared" peptides. We thus tested whether we could detect changes in the levels of Aquaporin-1, a water channel,[31] that was only identified with 1 "unique" peptide and no shared peptide (Supplementary Table S5). Based on proteomics results, we postulated that Aquaporin-1 would be upregulated in LE/Lys samples of JNCL patients and NPC patients compared to controls. We confirmed this upregulation by western blot (Supplementary Fig. S4). This result supports the robustness of our differentially expressed proteins results that were obtained with a more stringent filter.

First, we analysed the proteins shared by LE/Lys samples of controls and JNCL patients. We found that out of 6223 proteins detected in both JNCL and controls, 1683 proteins were differentially expressed (multiple t-tests p value with permutation-based FDR correction <0.05). We further analysed the 975 proteins which were upregulated and the 487 proteins which were downregulated by more than 1.5 fold (Supplementary Table S6 and Supplementary Fig. S5). We performed GO category enrichment analysis on proteins upregulated in JNCL samples compared to controls (Fig. 3a and Supplementary Table S7). The most significantly enriched biological process GO pathways were regulated exocytosis, exocytosis and secretion, as well as organic acid, oxoacid and carboxylic acid metabolic process. Pathways linked to immunity such as leukocyte degranulation, neutrophil mediated immunity and neutrophil activation involved in immune response were also enriched. At the molecular function level, we found an enrichment in pathways of cell adhesion molecule binding, cadherin binding, protein-containing complex binding, cytoskeletal protein binding, actin binding, lipid binding and phospholipid binding. Ligase and oxidoreductase activity pathways were also enriched. KEGG analysis revealed that metabolic pathways were highly enriched. We also observed that lysosome, regulation of actin cytoskeleton and propanoate, glycine, serine and threonine as well as carbon metabolism pathways were significantly enriched.

We then performed similar enrichment analysis on the 487 proteins downregulated in JNCL LE/Lys compared to controls (Fig. 3b and Supplementary Table S8). The most significantly enriched biological process GO pathways were chemical synaptic transmission, anterograde trans-synaptic signalling, trans-synaptic signalling and synaptic signalling pathways. We also observed an enrichment in the ion, cation, inorganic cation and metal ion transmembrane transporter activities pathways, as well as in the voltage-gated cation channel activity pathway. The glutamatergic synapse and synaptic vesicle cycle KEGG pathways were also highly enriched.

We also analysed the 6011 proteins shared by LE/Lys samples of controls and NPC patients and found that, amongst them, 1611 proteins were differentially expressed (multiple t-tests p value with permutation-based FDR correction <0.05), including 1358 that showed fold change of more than 1.5 (Supplementary Table S9 and Supplementary Fig. S6). We first performed GO enrichment analysis on the 848 proteins upregulated by more than 1.5 fold in NPC LE/Lys

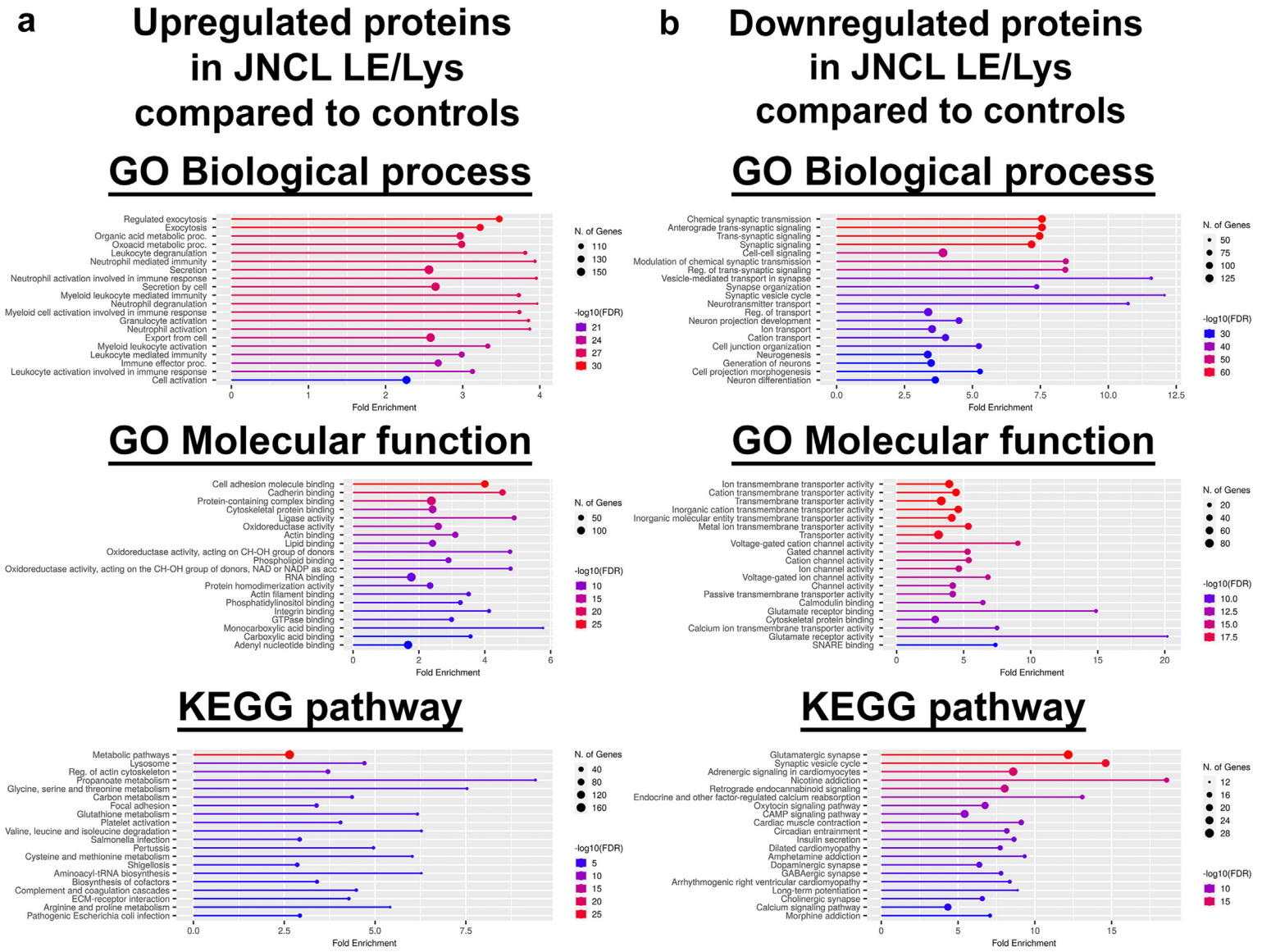


***Fig. 3*: Gene ontology (GO) analysis of differentially expressed proteins in JNCL LE/Lys samples compared to controls. a,** upregulated proteins. **b,** downregulated proteins. Significantly changed protein abundance was determined by multiple t-tests with a threshold for significance of $p < 0.05$ (with a permutation-based FDR correction). Only proteins that were upregulated or downregulated by more than 1.5 fold change (FC) were considered for analysis. GO enrichment was significant with FDR<1%.

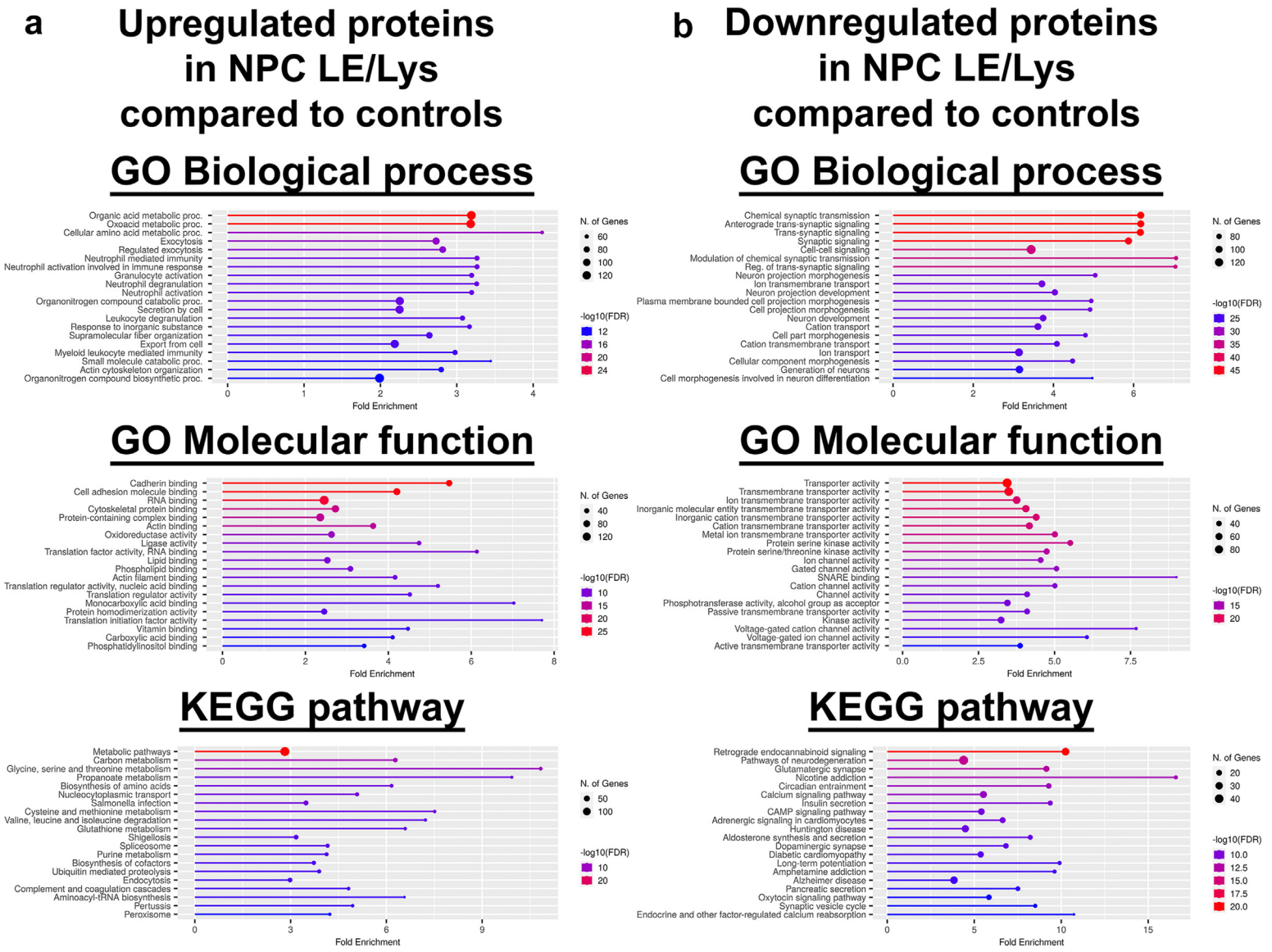


***Fig. 4:*** **Gene ontology (GO) analysis of differentially expressed proteins in NPC LE/Lys samples compared to controls. a,** upregulated proteins. **b,** downregulated proteins. Significantly changed protein abundance was determined by multiple t-tests with a threshold for significance of $p < 0.05$ (with a permutation-based FDR correction). Only proteins that were upregulated or downregulated by more than 1.5 fold change (FC) were considered for analysis. GO enrichment was significant with FDR<1%.

compared to controls (Fig. 4a and Supplementary Table S10). The most significantly enriched pathways were organic acid, carboxylic acid, oxoacid and cellular amino acid metabolic process pathways. The exocytosis and regulated exocytosis pathways were also enriched as well as the neutrophil mediated immunity, neutrophil activation involved in immune response, granulocyte activation and neutrophil degranulation pathways. In terms of molecular function, the most significantly enriched pathways were cadherin binding, cell adhesion molecule binding, RNA binding, cytoskeletal protein binding, protein-containing complex binding, actin binding and lipid binding. The oxidoreductase and ligase activity pathways were also enriched. The KEGG metabolic pathways were particularly enriched, in particular carbon metabolism, glycine, serine and threonine metabolism, propanoate metabolism and biosynthesis of amino acids.

We then analysed the 510 proteins downregulated by more than 1.5 fold in NPC LE/Lys compared to controls (Fig. 4b and Supplementary Table S11). The most significantly enriched biological process GO pathways were chemical synaptic transmission, anterograde trans-synaptic signalling, trans-synaptic signalling and synaptic signalling. Transporter and transmembrane transporter activity pathways, as well as inorganic molecular entity, ion, inorganic cation, cation and metal ion transmembrane transporter activity pathways were also enriched. In addition, KEGG pathways associated with retrograde endocannabinoid signalling, neurodegeneration and glutamatergic synapse also showed a significant enrichment.

We also performed a pathway analysis on proteins differentially expressed in JNCL LE/Lys compared to controls (Table 1 and Fig. 5a) as well as in NPC LE/Lys compared to controls (Table 2 and Fig. 5b). For both analyses, the functional pathways overrepresented in upregulated proteins were linked to immunity and response to stress while the functional pathways overrepresented in downregulated proteins were linked to synaptic function. As already suggested by our GO enrichment analysis, proteins differentially expressed in JNCL LE/Lys compared to controls displayed significant functional similarities with proteins differentially expressed in NPC LE/Lys. Indeed, upregulated proteins shared three and downregulated proteins shared nine of the ten most overrepresented pathways, respectively (Table 1 and 2).

Finally, we analysed the 6111 proteins shared by LE/Lys samples of JNCL and NPC patients. Strikingly, we observed that there was only one protein differentially expressed between JNCL and NPC samples (multiple t-tests p value with permutation-based FDR correction <0.05) (Supplementary Table S12 and Supplementary

| **Proteins upregulated in JNCL LE/Lys vs. controls** | | | |
|---|---|---|---|
| Pathway name | Number of genes observed | Number of genes in the pathway | Enrichment FDR |
| **Neutrophil degranulation** | 102 | 480 | $1.97\ 10^{-13}$ |
| Immune system | 290 | 2703 | $8.46\ 10^{-07}$ |
| **Innate immune system** | 166 | 1345 | $8.46\ 10^{-07}$ |
| ER-Phagosome pathway | 40 | 173 | $8.99\ 10^{-07}$ |
| Antigen processing-Cross presentation | 42 | 195 | $2.13\ 10^{-06}$ |
| Class I MHC mediated antigen processing & presentation | 71 | 479 | $6.20\ 10^{-05}$ |
| Interferon signaling | 62 | 397 | $6.20\ 10^{-05}$ |
| **Nuclear events mediated by NFE2L2** | 26 | 110 | $1.91\ 10^{-04}$ |
| Response to elevated platelet cytosolic Ca2+ | 31 | 148 | $1.97\ 10^{-04}$ |
| Platelet degranulation | 29 | 141 | $5.34\ 10^{-04}$ |
| **Proteins downregulated in JNCL LE/Lys vs. controls** | | | |
| Pathway name | Number of genes observed | Number of genes in the pathway | Enrichment FDR |
| **Neurexins and neuroligins** | 29 | 60 | $1.68\ 10^{-14}$ |
| **Protein-protein interactions at synapses** | 38 | 93 | $1.68\ 10^{-14}$ |
| **Neurotransmitter receptors and postsynaptic signal transmission** | 46 | 232 | $1.68\ 10^{-14}$ |
| **Neuronal system** | 104 | 490 | $1.68\ 10^{-14}$ |
| **Transmission across chemical synapses** | 68 | 344 | $1.68\ 10^{-14}$ |
| **Trafficking of AMPA receptors** | 17 | 37 | $5.90\ 10^{-12}$ |
| **Glutamate binding, activation of AMPA receptors and synaptic plasticity** | 17 | 39 | $1.16\ 10^{-11}$ |
| **Unblocking of NMDA receptors, glutamate binding and activation** | 14 | 27 | $1.56\ 10^{-10}$ |
| **LGI-ADAM interactions** | 11 | 14 | $4.32\ 10^{-10}$ |
| Serotonin Neurotransmitter Release Cycle | 11 | 23 | $6.95\ 10^{-08}$ |

Bold type indicates pathways that were also found overrepresented in the NPC vs. control analysis.

*Table 1:* **Overrepresented functional pathways in proteins differentially expressed in JNCL compared to control LE/Lys samples.**

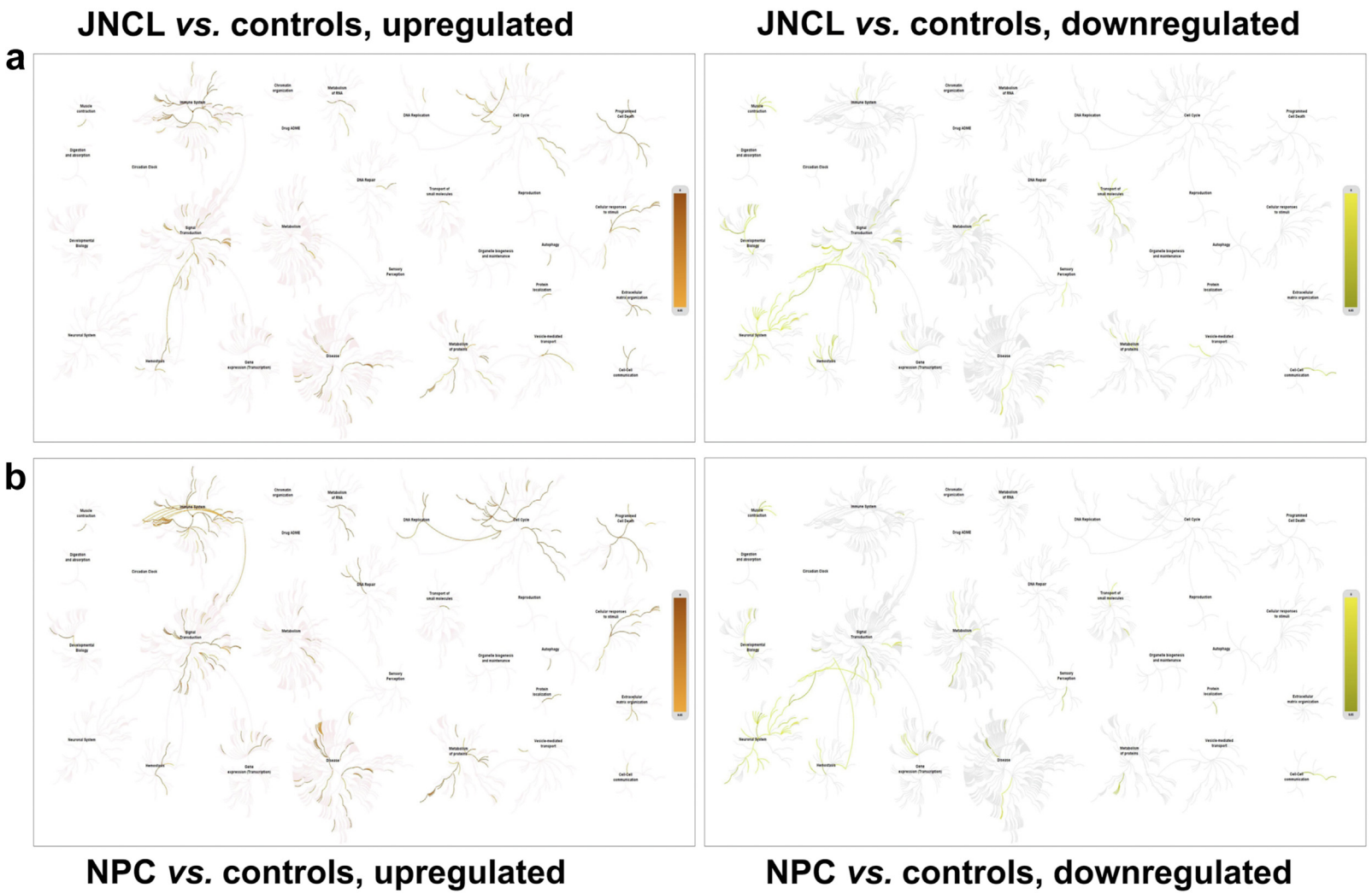


***Fig. 5:*** **Overrepresented functional pathways in differentially expressed proteins. a**, JNCL vs. control samples. Left panel, upregulated proteins. Right panel, downregulated proteins. **b**, NPC vs. control samples. Left panel, upregulated proteins. Right panel, downregulated proteins. Representation was generated with reactome.org.

| Proteins upregulated in NPC LE/Lys vs. controls | | | |
|---|---|---|---|
| Pathway name | Number of genes observed | Number of genes in the pathway | Enrichment FDR |
| **Neutrophil degranulation** | 79 | 480 | $9.91\ 10^{-10}$ |
| Programmed Cell Death | 47 | 237 | $8.56\ 10^{-08}$ |
| **Innate Immune System** | 150 | 1345 | $2.68\ 10^{-07}$ |
| Apoptosis | 40 | 192 | $2.68\ 10^{-07}$ |
| Neddylation | 43 | 254 | $1.59\ 10^{-05}$ |
| **Nuclear events mediated by NFE2L2** | 26 | 110 | $1.59\ 10^{-05}$ |
| Regulation of mRNA stability by proteins that bind AU-rich elements | 23 | 93 | $3.57\ 10^{-05}$ |
| KEAP1-NFE2L2 pathway | 29 | 146 | $6.71\ 10^{-05}$ |
| AUF1 (hnRNP D0) binds and destabilizes mRNA | 17 | 56 | $6.71\ 10^{-05}$ |
| Vif-mediated degradation of APOBEC3G | 17 | 56 | $6.71\ 10^{-05}$ |
| **Proteins downregulated in NPC LE/Lys vs. controls** | | | |
| Pathway name | Number of genes observed | Number of genes in the pathway | Enrichment FDR |
| **Protein–protein interactions at synapses** | 29 | 93 | $4.75\ 10^{-14}$ |
| **Neuronal system** | 82 | 490 | $4.75\ 10^{-14}$ |
| **Transmission across chemical synapses** | 50 | 344 | $6.33\ 10^{-14}$ |
| **Neurotransmitter receptors and postsynaptic signal transmission** | 39 | 232 | $1.14\ 10^{-12}$ |
| **Neurexins and neuroligins** | 21 | 60 | $3.23\ 10^{-12}$ |
| **Trafficking of AMPA receptors** | 16 | 37 | $1.56\ 10^{-10}$ |
| **Glutamate binding, activation of AMPA receptors and synaptic plasticity** | 16 | 39 | $2.84\ 10^{-10}$ |
| **Unblocking of NMDA receptors, glutamate binding and activation** | 14 | 27 | $2.84\ 10^{-10}$ |
| Long-term potentiation | 12 | 31 | $2.37\ 10^{-07}$ |
| **LGI-ADAM interactions** | 9 | 14 | $2.92\ 10^{-07}$ |

Bold type indicates pathways that were also found overrepresented in the JNCL vs. control analysis.

*Table 2:* **Overrepresented functional pathways in proteins differentially expressed in NPC compared to control LE/Lys samples.**

Fig. S7). We found that NPC1 was upregulated by ~6.5 fold in JNCL samples, compared to NPC samples. *NPC1* is one of the genes mutated in NPC disease and codes a protein that resides in the limiting membrane of LE/Lys where it plays a role in the intracellular trafficking of cholesterol. It has been described that some disease-causing mutations in *NPC1* can cause the protein to be mislocalized away from LE/Lys.[32]

## Discussion

Our results support that juvenile CLN3 disease, the most common form of NCL, is a lysosomal cholesterol storage disorder, reminiscent of phenotypes observed in NPC disease. In this study, we have analysed in an unbiased manner the lipid and protein landscape of LE/Lys isolated from the cortex of JNCL patients and compared them with unaffected controls and NPC disease patients. We have found that cholesterol, among other lipids, accumulates in the LE/Lys of JNCL patients compared to unaffected controls. We have also observed that this accumulation is comparable to the expected accumulation of cholesterol in LE/Lys of NPC patients. Lipid profiles in LE/Lys of JNCL and NPC patients were similar, except for levels of BMP. Protein profiles in LE/Lys of JNCL and NPC patients were also comparable, except for levels of NPC1. Taken together, our results support that JNCL and NPC share pathways leading to aberrant lysosomal accumulation of lipids and proteins.

Although we cannot fully rule out minor contributions from contaminants and inter-organelle contacts, our immunoprecipitation fractions were highly enriched in intact LE/Lys, as assessed by western blot, TEM and proteomics. We found that LE/Lys accumulated cholesterol and GM3 in the brains of JNCL patients as compared to controls. Conversely, in comparison with controls, LE/Lys of JNCL patients were depleted of phosphatidylcholine, ether phosphatidylcholine, sphingomyelin, phosphatidylethanolamine, phosphatidylserine, ceramides and phosphatidylglycerol. We believe that a lipidomics analysis of human LE/Lys from JNCL brain tissues has not been performed so far. However, some previous studies investigated lipid changes at the whole brain level in JNCL patients. A report suggested increased ceramides levels in JNCL brains compared to controls,[33] while another indicated that lipids from JNCL brains were overall similar to controls.[34] Another study isolated detergent resistant membranes (DRMs) from the plasma membrane and LE and found that levels of BMP were decreased in DRMs isolated from JNCL brains.[35] A recent study analysed the lipidomics profile of LE/Lys isolated from a mouse model of JNCL and found that BMP was decreased while lysophosphatidylglycerol (LPG) was

| Gene name | Protein name | SwissProt ID | p value | log2 fold change | Protein description |
|---|---|---|---|---|---|
| NPC2 | NPC2_HUMAN | not detected in JNCL or control samples | | | NPC intracellular cholesterol transporter 2 |
| IGF2R | MPRI_HUMAN | not detected in JNCL samples | | | Cation-independent mannose-6-phosphate receptor |
| Retromer complex | | | | | |
| VPS26A | VP26A_HUMAN | O75436 | 0.035 | 0.96 | Vacuolar protein sorting-associated protein 26 A |
| VPS29 | VPS29_HUMAN | Q9UBQ0; Q9UBQ0-2 | 0.036 | 1.21 | Vacuolar protein sorting-associated protein 29 |
| SNX2 | SNX2_HUMAN | O60749; O60749-2 | 0.0062 | 1.14 | Sorting nexin-2 |
| SNX5 | SNX5_HUMAN | Q9Y5X3 | 0.046 | 0.68 | Sorting nexin-5 |
| SNX6 | SNX6_HUMAN | Q9UNH7; Q9UNH7-2 | 0.0079 | 1.08 | Sorting nexin-6 |
| Mannose-6-phosphate containing proteins | | | | | |
| ASAH1 | ASAH1_HUMAN | Q13510; Q13510-2; Q13510-3 | 0.0022 | 1.55 | Acid ceramidase |
| PPT1 | PPT1_HUMAN | P50897; P50897-2 | 0.0022 | 2.38 | Palmitoyl-protein thioesterase 1 |
| TPP1 | TPP1_HUMAN | O14773; O14773-2 | 0.0080 | 2.60 | Tripeptidyl-peptidase 1 |
| CTSD | CATD_HUMAN | P07339 | 0.0078 | 0.80 | Cathepsin D |
| GAA | LYAG_HUMAN | P10253 | 0.045 | 1.24 | Lysosomal alpha-glucosidase |
| LIPA | LICH_HUMAN | P38571; P38571-2 | 0.0067 | 1.28 | Lysosomal acid lipase/cholesteryl ester hydrolase |
| PSAP | SAP_HUMAN | P07602; P07602-2; P07602-3 | 0.0024 | 3.09 | Prosaposin |
| CTSF | CATF_HUMAN | Q9UBX1 | 0.011 | 1.93 | Cathepsin F |
| CTSZ | CATZ_HUMAN | Q9UBR2 | 0.049 | 1.00 | Cathepsin Z |
| GGH | GGH_HUMAN | Q92820 | 0.0054 | 1.06 | Gamma-glutamyl hydrolase |
| V-ATPase subunits | | | | | |
| ATP6V0A1 | VPP1_HUMAN | Q93050; Q93050-1 | 0.0033 | −1.04 | V-type proton ATPase 116 kDa subunit a1 |
| ATP6V0C | VATL_HUMAN | P27449 | 0.024 | −0.73 | V-type proton ATPase 16 kDa proteolipid subunit |
| ATP6V0D1 | VA0D1_HUMAN | P61421 | 0.0024 | −1.12 | V-type proton ATPase subunit d 1 |
| ATP6V1B2 | VATB2_HUMAN | P21281 | 0.043 | −0.64 | V-type proton ATPase subunit B, brain isoform |
| ATP6V1G1 | VATG1_HUMAN | O75348 | 0.036 | 0.59 | V-type proton ATPase subunit G 1 |

A list of all detected proteins that were statistically different between control and JNCL samples (multiple t-tests p value with a permutation-based FDR correction <0.05) with a fold change ≥1.5 is presented in Supplementary Table S6.

***Table 3:*** **Subset of proteins differentially expressed in control and JNCL LE/Lys samples related to NPC2 trafficking.**

increased, compared to controls.[36] Cholesterol was not investigated in the latter study.

Based on our previous work,[14] and assuming that there is indeed a mistrafficking of CI-M6PR and NPC2 in JNCL as proposed in cellular models,[9–11] we expect overall cholesterol levels to be unaffected at the cellular/tissue level. However, we expect cholesterol to be redistributed, with an accumulation in the LE/Lys (as demonstrated in this study) and a potential decrease in other compartments, including the plasma membrane. This hypothesis will require further investigation but may explain why changes in cholesterol have not been described earlier in JNCL.

Intriguingly, it has been reported that LE/Lys have a more peripheral localisation in cellular models of JNCL.[37,38] As the positioning of LE/Lys depends on their cholesterol content,[39] the accumulation of cholesterol we demonstrate here may in part explain the LE/Lys positioning phenotype in JNCL cellular models.

A recent report failed to show a lysosomal cholesterol accumulation in human JNCL fibroblasts using filipin staining.[40] Lipofuscin deposition may interfere with filipin signal in this model. It is also possible that cholesterol may accumulate more readily in brain cell types than in fibroblasts. Of note, the authors used human cortical neurons derived from JNCL induced pluripotent stem cells (iPSCs) in their study but did not investigate cholesterol in these cells.

As we were able to demonstrate a cholesterol increase in the LE/Lys of JNCL patients compared to controls, we decided to test our initial postulate that NPC2 levels are lower in JNCL samples using our proteomics results. However, we were not able to detect NPC2 in our proteomics assay in control nor in JNCL samples and thus could not make a solid conclusion (Table 3). It is likely that we were not able to detect NPC2 because levels of this protein were extremely low. We also looked at the receptor itself, the cation-independent M6PR (CI-M6PR, coded by *IGF2R*). Indeed, if *CLN3* mutations cause CI-M6PR to be mistrafficked and blocked in the trans-Golgi network (TGN),[9] we would expect to find lower levels of the receptor in LE/Lys of JNCL samples compared to controls. However, we observed that although CI-M6PR was detected in control samples, it was not detected in JNCL samples (Table 3). This does not invalidate our hypothesis yet precludes us from drawing robust conclusions. The cation-dependent M6PR (CD-M6PR, coded by *M6PR*) was not detected in our samples.

A key protagonist in CI-M6PR trafficking is the retromer complex, which is responsible for the retrograde transport of CI-M6PR from the endosomes to the TGN.[41] Importantly, it was reported that CLN3 plays an important role in retromer function (reviewed in[8]). We thus investigated whether components of the retromer were differentially expressed in JNCL LE/Lys compared to controls. We found that two subunits of the retromer cargo-selective core subcomplex, Vps26 A and Vps29, were upregulated in JNCL samples (Table 3). We also investigated the retromer membrane-deforming subcomplex, composed of a sorting nexin (SNX) heterodimer, and involved in tubulo-vesicular carrier formation from endosomal membranes and observed that three of the four SNXs involved in CI-M6PR transport (SNX2, SNX5 and SNX6) were upregulated in JNCL LE/Lys samples (Table 3). Altogether, subunits of the retromer complex aberrantly accumulate in JNCL LE/Lys, supporting that retromer may be affected in JNCL, with potential consequences on CI-M6PR trafficking.

In addition, we investigated other brain proteins containing a mannose-6-phosphate group[42] to test whether we could see a clear trend in the level of these cargoes in LE/Lys of JNCL patients compared to controls. We found that multiple cargoes (e.g., cathepsin D, prosaposin) were upregulated in JNCL LE/Lys (Table 3). However, some aspects of lysosomal biology need to be taken into account before making conclusions. Indeed, most of these mannose-6-phosphate proteins are pre-proproteins that need to be cleaved to become active, and this cleavage depends on correct lysosomal pH environment and function. An increase in these cargoes could thus result from increased delivery to the LE/Lys or from a defect in their processing due to inadequate lysosomal pH. Furthermore, even though human brain tissues are a powerful tool to gain insight into potential pathogenic mechanisms, they are not dynamic and do not allow us to differentiate between e.g., an initial defect in cargo loading in LE/Lys and secondary accumulations due to lysosomal dysfunction further in the progression of the disease. This is particularly significant here, where multiple key subunits of the V-ATPase are downregulated in JNCL LE/Lys compared to controls (Table 3), strongly suggesting that lysosomal pH may be affected in JNCL, as previously proposed in model systems.[43–47] Taking all these aspects into consideration, we were not able to make a solid conclusion regarding mannose-6-phosphate containing proteins in human brain samples in JNCL patients.

If we incorporate our findings with results from model systems and postulate that model systems correspond to early stages of the disease, while we are looking at the end point, we can propose that mutations in *CLN3* lead to mistrafficking of CI-M6PR and NPC2 and initial triggering of lysosomal cholesterol accumulation. Over time, this could cause more general lysosomal dysfunction and secondary accumulation of enzymes such as lysosomal acid lipase (LIPA), that extracts free cholesterol from cholesterol esters, which would further exacerbate the cholesterol accumulation phenotype.

The only lipid class that showed differences between JNCL and NPC LE/Lys is BMP (also called lysobisphosphatidic acid or LBPA), a lipid uniquely localised to LE/Lys, where it is further concentrated in intralumenal vesicles (ILVs).[48] BMP has been proposed to control the cholesterol storage capacity of LE/Lys and subsequently, intracellular cholesterol levels.[49,50] This lipid also affects the correct sorting and degradation of proteins and lipids. In particular, it plays a key role in the trafficking of CI-M6PR[48] and facilitates the correct degradation of sphingolipids.[51] BMP levels have been reported to be decreased in JNCL patients samples as well as in murine and cellular models of the disease[35,36] and CLN3 has been proposed to control BMP synthesis.[35] We recently reported that lysosomal phospholipase A2 contributes to the biosynthesis of BMP[52] but we were unable to detect this enzyme in our samples. The mechanisms underlying the differential regulation of BMP levels in JNCL and NPC warrant further investigation.

We also performed a proteomic analysis of LE/Lys isolated from JNCL patients' brains. It is noteworthy that the proteins downregulated in JNCL compared to controls were highly enriched in pathways linked to synaptic function and that this was recapitulated in proteins downregulated in NPC compared to controls. The relationship between the aberrant accumulation of proteins and lipids in the LE/Lys and synaptic dysfunction, although commonly observed in lysosomal storage disorders, is still incompletely understood at the mechanistic level.[53] CLN3 has been proposed to be present in synaptosomes[54] and recent studies in JNCL model systems support that neuronal network dysfunction and synaptic alterations may in fact precede aberrant LE/Lys storage.[55,56] We observed that proteins downregulated in JNCL LE/Lys compared to controls were associated with the glutamatergic and GABAergic synapse KEGG pathways. This is in good accordance with previous reports of dysfunction of glutamate and GABA currents in JNCL model systems (e.g.,[57–59]).

Unexpectedly, we observed that among the LE/Lys proteins detected in both JNCL and NPC, only one protein, NPC1, was differentially expressed. Thus, although they are caused by mutations in two separate genes, JNCL and NPC result in the lysosomal accumulation of the same proteins. As mutations in *NPC1* are the most common cause of NPC disease and since it has been described that some disease-causing mutations in *NPC1* can cause the protein to be mislocalized away from LE/Lys,[32] it is not surprising that levels of NPC1 would be decreased in NPC patients compared to JNCL patients.

Our study establishes similarities in the lipids and proteins accumulated in the LE/Lys of patients with JNCL and NPC. These disorders are caused by mutations in different genes and differ in their presentation. However, their similarities at the LE/Lys level suggest that they may share some pathogenic pathways. It is thus possible that therapeutic treatments currently available or being tested for NPC patients may also be beneficial to JNCL patients. Additional studies in cellular and murine models of JNCL[60–62] will be necessary to answer this important question.

Another angle to consider when analysing our results are the many parallels being drawn between lysosomal storage disorders and neurodegenerative disorders of ageing. Examples include not only Gaucher and Parkinson's diseases, but also NPC and Alzheimer's diseases. Indeed, NPC patients present with intracellular accumulation of APP fragments,[63] as well as neurofibrillary tangles of tau that are similar to Alzheimer's disease.[64] Evidence also points towards similarities between JNCL and neurodegenerative disorders of ageing. For example, accumulation of intracellular APP fragments has been described in the brains of JNCL patients[65] and altered processing of APP has been reported in JNCL cellular models.[44] In addition, it was reported that JNCL patients display elevated levels of tau in their cerebrospinal fluid.[66] *CLN3* has also been associated with the risk of developing early onset Alzheimer's disease.[67] However, JNCL patients also often present with Parkinsonism[2] and JNCL cellular models display increased levels of α-synuclein oligomers.[68] We thus suggest that similarities between JNCL and Alzheimer's disease, Parkinson's disease or both should be further investigated in the future.

Taken together, our results support that juvenile CLN3 disease, the most common form of NCL, is a lysosomal cholesterol storage disorder with previously unsuspected similarities with NPC disease. The parallels we draw between these two disorders shed new light on the mechanistic pathways underlying JNCL pathogenesis and pave the way for novel therapeutic perspectives for JNCL patients.

#### Contributors

C.M. conceived the research. J.C., Y.X., L.D., S.S., R.H.Jr., J.M., R.K.S. and C.M. performed and analysed the experiments. B.V. analysed the sequencing data. J.H.L., E.A.-G., R.N., F.-X.L. and C.M. oversaw the experiments. C.M. wrote the manuscript. All authors edited the manuscript. All authors read and approved the final version of the manuscript.

Lipidomics data were verified by members of the lipidomics core (Y.X., L.D., R.N.) as well as J.C. and C.M. Proteomics data were verified by R.K.S. and C.M. TEM data were verified by F.-X.L., S.S. and C.M. western blot data were verified by J.C., R.H.Jr. and C.M.

#### Data sharing statement

All data collected during this study are included in this article (and its supplementary information files). Proteomics raw data have been deposited in the MassIVE database (MSV000091428). Additional information relating to the methodologies used in this study will be provided upon request.

#### Declaration of interests

The authors declare no competing financial interests.

#### Acknowledgements

We are grateful to the CLN3 disease families and their physicians for making this research effort possible. We thank the NIH NeuroBioBank for providing us with human tissue samples. We acknowledge NYULH DART Microscopy Lab Kristen Dancel-Manning for her assistance with EM work. This core is partially supported by Laura and Isaac Perlmutter Cancer Center Support Grant NIH/NCI P30CA016087. Lipidomics analysis was performed in the Biomarkers Core Laboratory at the Irving Institute for Clinical and Translational Research at Columbia University Irving Medical Center. Proteomics analysis was performed in the Proteomics and Macromolecular Crystallography Shared Resource in the Herbert Irving Comprehensive Cancer Center at Columbia University Irving Medical Center. Next generation sequencing and PCR tests were performed in the Center for Applied Genomics of the Children's Hospital of Philadelphia. The work was supported by a grant from the San Francisco Foundation to C.M. The funding source had no involvement in the collection, analysis and interpretation of the data, nor in the writing of the manuscript.

#### Appendix A. Supplementary data

Supplementary data related to this article can be found at https://doi.org/10.1016/j.ebiom.2023.104628.

#### References

1 Carcel-Trullols J, Kovacs AD, Pearce DA. Cell biology of the NCL proteins: what they do and don't do. *Biochim Biophys Acta*. 2015;1852(10 Pt B):2242–2255.
2 Mole SE, Anderson G, Band HA, et al. Clinical challenges and future therapeutic approaches for neuronal ceroid lipofuscinosis. *Lancet Neurol*. 2019;18(1):107–116.
3 Gardner E, Mole SE. The genetic basis of phenotypic heterogeneity in the neuronal ceroid lipofuscinoses. *Front Neurol*. 2021;12:754045.
4 Williams RE, Mole SE. New nomenclature and classification scheme for the neuronal ceroid lipofuscinoses. *Neurology*. 2012;79(2):183–191.
5 Isolation of a novel gene underlying batten disease, CLN3. The international batten disease consortium. *Cell*. 1995;82(6):949–957.
6 Masten MC, Williams JD, Vermilion J, et al. The CLN3 Disease Staging System: a new tool for clinical research in Batten disease. *Neurology*. 2020;94(23):e2436–e2440.
7 Mirza M, Vainshtein A, DiRonza A, et al. The CLN3 gene and protein: what we know. *Mol Genet Genomic Med*. 2019;7(12):e859.
8 Cotman SL, Lefrancois S. CLN3, at the crossroads of endocytic trafficking. *Neurosci Lett*. 2021;762:136117.
9 Metcalf DJ, Calvi AA, Seaman M, Mitchison HM, Cutler DF. Loss of the Batten disease gene CLN3 prevents exit from the TGN of the mannose 6-phosphate receptor. *Traffic*. 2008;9(11):1905–1914.
10 Schmidtke C, Tiede S, Thelen M, et al. Lysosomal proteome analysis reveals that CLN3-defective cells have multiple enzyme deficiencies associated with changes in intracellular trafficking. *J Biol Chem*. 2019;294(24):9592–9604.
11 Yasa S, Modica G, Sauvageau E, Kaleem A, Hermey G, Lefrancois S. CLN3 regulates endosomal function by modulating Rab7A-effector interactions. *J Cell Sci*. 2020;133(6):jcs234047.
12 Willenborg M, Schmidt CK, Braun P, et al. Mannose 6-phosphate receptors, Niemann-Pick C2 protein, and lysosomal cholesterol accumulation. *J Lipid Res*. 2005;46(12):2559–2569.
13 Rosenbaum AI, Maxfield FR. Niemann-Pick type C disease: molecular mechanisms and potential therapeutic approaches. *J Neurochem*. 2011;116(5):789–795.
14 Marquer C, Tian H, Yi J, et al. Arf6 controls retromer traffic and intracellular cholesterol distribution via a phosphoinositide-based mechanism. *Nat Commun*. 2016;7:11919.
15 Bolton SC, Soran V, Marfa MP, et al. Clinical disease characteristics of patients with Niemann-Pick disease type C: findings from the

international Niemann-Pick disease registry (INPDR). *Orphanet J Rare Dis*. 2022;17(1):51.
16 Cohen J. *Statistical power analysis for the behavioral sciences*. New Jersey: Lawrence Erlbaum Assoc.; 1987.
17 Taschner PE, de Vos N, Breuning MH. Rapid detection of the major deletion in the Batten disease gene CLN3 by allele specific PCR. *J Med Genet*. 1997;34(11):955–956.
18 Agudelo CW, Kumley BK, Area-Gomez E, et al. Decreased surfactant lipids correlate with lung function in chronic obstructive pulmonary disease (COPD). *PLoS One*. 2020;15(2):e0228279.
19 Area-Gomez E, Larrea D, Yun T, et al. Lipidomics study of plasma from patients suggest that ALS and PLS are part of a continuum of motor neuron disorders. *Sci Rep*. 2021;11(1):13562.
20 Chan RB, Oliveira TG, Cortes EP, et al. Comparative lipidomic analysis of mouse and human brain with Alzheimer disease. *J Biol Chem*. 2012;287(4):2678–2688.
21 Guan Z, Li S, Smith DC, Shaw WA, Raetz CR. Identification of N-acylphosphatidylserine molecules in eukaryotic cells. *Biochemistry*. 2007;46(50):14500–14513.
22 Hsu FF, Turk J, Shi Y, Groisman EA. Characterization of acylphosphatidylglycerols from Salmonella typhimurium by tandem mass spectrometry with electrospray ionization. *J Am Soc Mass Spectrom*. 2004;15(1):1–11.
23 Kulak NA, Pichler G, Paron I, Nagaraj N, Mann M. Minimal, encapsulated proteomic-sample processing applied to copy-number estimation in eukaryotic cells. *Nat Methods*. 2014;11(3):319–324.
24 Meier F, Brunner AD, Frank M, et al. diaPASEF: parallel accumulation-serial fragmentation combined with data-independent acquisition. *Nat Methods*. 2020;17(12):1229–1236.
25 Demichev V, Messner CB, Vernardis SI, Lilley KS, Ralser M. DIA-NN: neural networks and interference correction enable deep proteome coverage in high throughput. *Nat Methods*. 2020;17(1):41–44.
26 Tyanova S, Temu T, Sinitcyn P, et al. The perseus computational platform for comprehensive analysis of (prote)omics data. *Nat Methods*. 2016;13(9):731–740.
27 Ge SX, Jung D, Yao R. ShinyGO: a graphical gene-set enrichment tool for animals and plants. *Bioinformatics*. 2020;36(8):2628–2629.
28 Fabregat A, Sidiropoulos K, Viteri G, et al. Reactome diagram viewer: data structures and strategies to boost performance. *Bioinformatics*. 2018;34(7):1208–1214.
29 Tindi JO, Chavez AE, Cvejic S, Calvo-Ochoa E, Castillo PE, Jordan BA. ANKS1B gene product AIDA-1 controls hippocampal synaptic transmission by regulating GluN2B subunit localization. *J Neurosci*. 2015;35(24):8986–8996.
30 Younis RM, Taylor RM, Beardsley PM, McClay JL. The ANKS1B gene and its associated phenotypes: focus on CNS drug response. *Pharmacogenomics*. 2019;20(9):669–684.
31 Xu M, Xiao M, Li S, Yang B. Aquaporins in nervous system. *Adv Exp Med Biol*. 2017;969:81–103.
32 Shammas H, Kuech EM, Rizk S, Das AM, Naim HY. Different niemann-pick C1 genotypes generate protein phenotypes that vary in their intracellular processing, trafficking and localization. *Sci Rep*. 2019;9(1):5292.
33 Puranam K, Qian WH, Nikbakht K, et al. Upregulation of Bcl-2 and elevation of ceramide in Batten disease. *Neuropediatrics*. 1997;28(1):37–41.
34 Kakela R, Somerharju P, Tyynela J. Analysis of phospholipid molecular species in brains from patients with infantile and juvenile neuronal-ceroid lipofuscinosis using liquid chromatography-electrospray ionization mass spectrometry. *J Neurochem*. 2003;84(5):1051–1065.
35 Hobert JA, Dawson G. A novel role of the Batten disease gene CLN3: association with BMP synthesis. *Biochem Biophys Res Commun*. 2007;358(1):111–116.
36 Laqtom NN, Dong W, Medoh UN, et al. CLN3 is required for the clearance of glycerophosphodiesters from lysosomes. *Nature*. 2022;609(7929):1005–1011.
37 Fossale E, Wolf P, Espinola JA, et al. Membrane trafficking and mitochondrial abnormalities precede subunit c deposition in a cerebellar cell model of juvenile neuronal ceroid lipofuscinosis. *BMC Neurosci*. 2004;5:57.
38 Lojewski X, Staropoli JF, Biswas-Legrand S, et al. Human iPSC models of neuronal ceroid lipofuscinosis capture distinct effects of TPP1 and CLN3 mutations on the endocytic pathway. *Hum Mol Genet*. 2014;23(8):2005–2022.
39 Rocha N, Kuijl C, van der Kant R, et al. Cholesterol sensor ORP1L contacts the ER protein VAP to control Rab7-RILP-p150 Glued and late endosome positioning. *J Cell Biol*. 2009;185(7):1209–1225.
40 Scotto Rosato A, Krogsaeter EK, Jaslan D, et al. TPC2 rescues lysosomal storage in mucolipidosis type IV, Niemann-Pick type C1, and Batten disease. *EMBO Mol Med*. 2022;14(9):e15377.
41 Seaman MN. Cargo-selective endosomal sorting for retrieval to the golgi requires retromer. *J Cell Biol*. 2004;165(1):111–122.
42 Sleat DE, Lackland H, Wang Y, et al. The human brain mannose 6-phosphate glycoproteome: a complex mixture composed of multiple isoforms of many soluble lysosomal proteins. *Proteomics*. 2005;5(6):1520–1532.
43 Pearce DA, Nosel SA, Sherman F. Studies of pH regulation by Btn1p, the yeast homolog of human Cln3p. *Mol Genet Metab*. 1999;66(4):320–323.
44 Golabek AA, Kida E, Walus M, Kaczmarski W, Michalewski M, Wisniewski KE. CLN3 protein regulates lysosomal pH and alters intracellular processing of Alzheimer's amyloid-beta protein precursor and cathepsin D in human cells. *Mol Genet Metab*. 2000;70(3):203–213.
45 Holopainen JM, Saarikoski J, Kinnunen PK, Jarvela I. Elevated lysosomal pH in neuronal ceroid lipofuscinoses (NCLs). *Eur J Biochem*. 2001;268(22):5851–5856.
46 Gachet Y, Codlin S, Hyams JS, Mole SE. btn1, the Schizosaccharomyces pombe homologue of the human Batten disease gene CLN3, regulates vacuole homeostasis. *J Cell Sci*. 2005;118(Pt 23):5525–5536.
47 Vidal-Donet JM, Carcel-Trullols J, Casanova B, Aguado C, Knecht E. Alterations in ROS activity and lysosomal pH account for distinct patterns of macroautophagy in LINCL and JNCL fibroblasts. *PLoS One*. 2013;8(2):e55526.
48 Kobayashi T, Stang E, Fang KS, de Moerloose P, Parton RG, Gruenberg J. A lipid associated with the antiphospholipid syndrome regulates endosome structure and function. *Nature*. 1998;392(6672):193–197.
49 Kobayashi T, Beuchat MH, Lindsay M, et al. Late endosomal membranes rich in lysobisphosphatidic acid regulate cholesterol transport. *Nat Cell Biol*. 1999;1(2):113–118.
50 Chevallier J, Chamoun Z, Jiang G, et al. Lysobisphosphatidic acid controls endosomal cholesterol levels. *J Biol Chem*. 2008;283(41):27871–27880.
51 Gallala HD, Sandhoff K. Biological function of the cellular lipid BMP-BMP as a key activator for cholesterol sorting and membrane digestion. *Neurochem Res*. 2011;36(9):1594–1600.
52 Chen J, Cazenave-Gassiot A, Xu Y, et al. Lysosomal phospholipase A2 contributes to the biosynthesis of the atypical late endosome lipid bis(monoacylglycero)phosphate. *Commun Biol*. 2023;6(1):210.
53 Rebiai R, Givogri MI, Gowrishankar S, Cologna SM, Alford ST, Bongarzone ER. Synaptic function and dysfunction in lysosomal storage diseases. *Front Cell Neurosci*. 2021;15:619777.
54 Luiro K, Kopra O, Lehtovirta M, Jalanko A. CLN3 protein is targeted to neuronal synapses but excluded from synaptic vesicles: new clues to Batten disease. *Hum Mol Genet*. 2001;10(19):2123–2131.
55 Ahrens-Nicklas RC, Tecedor L, Hall AF, et al. Neuronal network dysfunction precedes storage and neurodegeneration in a lysosomal storage disorder. *JCI Insight*. 2019;4(21):e131961.
56 Gomez-Giro G, Arias-Fuenzalida J, Jarazo J, et al. Synapse alterations precede neuronal damage and storage pathology in a human cerebral organoid model of CLN3-juvenile neuronal ceroid lipofuscinosis. *Acta Neuropathol Commun*. 2019;7(1):222.
57 Pears MR, Cooper JD, Mitchison HM, Mortishire-Smith RJ, Pearce DA, Griffin JL. High resolution 1H NMR-based metabolomics indicates a neurotransmitter cycling deficit in cerebral tissue from a mouse model of Batten disease. *J Biol Chem*. 2005;280(52):42508–42514.
58 Kovacs AD, Pearce DA. Attenuation of AMPA receptor activity improves motor skills in a mouse model of juvenile Batten disease. *Exp Neurol*. 2008;209(1):288–291.
59 Grunewald B, Lange MD, Werner C, et al. Defective synaptic transmission causes disease signs in a mouse model of juvenile neuronal ceroid lipofuscinosis. *Elife*. 2017;6:e28685.
60 Kovacs AD, Pearce DA. Finding the most appropriate mouse model of juvenile CLN3 (Batten) disease for therapeutic studies: the importance of genetic background and gender. *Dis Model Mech*. 2015;8(4):351–361.
61 Minnis CJ, Thornton CD, FitzPatrick LM, McKay TR. Cellular models of Batten disease. *Biochim Biophys Acta Mol Basis Dis*. 2020;1866(9):165559.
62 Morsy A, Carmona AV, Trippier PC. Patient-derived induced pluripotent stem cell models for phenotypic screening in the neuronal ceroid lipofuscinoses. *Molecules*. 2021;26(20):6235.
63 Jin LW, Shie FS, Maezawa I, Vincent I, Bird T. Intracellular accumulation of amyloidogenic fragments of amyloid-beta

precursor protein in neurons with Niemann-Pick type C defects is associated with endosomal abnormalities. *Am J Pathol*. 2004;164(3):975–985.

64 Auer IA, Schmidt ML, Lee VM, et al. Paired helical filament tau (PHFtau) in Niemann-Pick type C disease is similar to PHFtau in Alzheimer's disease. *Acta Neuropathol*. 1995;90(6):547–551.

65 Wisniewski KE, Maslinska D, Kitaguchi T, Kim KS, Goebel HH, Haltia M. Topographic heterogeneity of amyloid B-protein epitopes in brains with various forms of neuronal ceroid lipofuscinoses suggesting defective processing of amyloid precursor protein. *Acta Neuropathol*. 1990;80(1):26–34.

66 Kay GW, Verbeek MM, Furlong JM, Willemsen MA, Palmer DN. Neuropeptide changes and neuroactive amino acids in CSF from humans and sheep with neuronal ceroid lipofuscinoses (NCLs, Batten disease). *Neurochem Int*. 2009;55(8):783–788.

67 Cheng R, Tang M, Martinez I, et al. Linkage analysis of multiplex Caribbean Hispanic families loaded for unexplained early-onset cases identifies novel Alzheimer's disease loci. *Alzheimers Dement (Amst)*. 2018;10:554–562.

68 Kang S, Heo TH, Kim SJ. Altered levels of alpha-synuclein and sphingolipids in Batten disease lymphoblast cells. *Gene*. 2014;539(2):181–185.